Accepted Manuscript

Short communication

Articular-surface-based automatic anatomical coordinate systems for the knee bones

Jean-Baptiste Renault, Gaëtan Aüllo-Rasser, Mathias Donnez, Sébastien Parratte, Patrick Chabrand

PII: S0021-9290(18)30710-3
DOI: https://doi.org/10.1016/j.jbiomech.2018.08.028
Reference: BM 8839

To appear in: *Journal of Biomechanics*

Accepted Date: 22 August 2018

Please cite this article as: J-B. Renault, G. Aüllo-Rasser, M. Donnez, S. Parratte, P. Chabrand, Articular-surface-based automatic anatomical coordinate systems for the knee bones, *Journal of Biomechanics* (2018), doi: https://doi.org/10.1016/j.jbiomech.2018.08.028

This is a PDF file of an unedited manuscript that has been accepted for publication. As a service to our customers we are providing this early version of the manuscript. The manuscript will undergo copyediting, typesetting, and review of the resulting proof before it is published in its final form. Please note that during the production process errors may be discovered which could affect the content, and all legal disclaimers that apply to the journal pertain.

ACCEPTED MANUSCRIPT

Articular-surface-based automatic anatomical coordinate systems for the knee bones.

Submitted as a Short Communication

Authors:
Jean-Baptiste RENAULT[a,b,*]

Gaëtan AÜLLO-RASSER[a,b,d]

Mathias DONNEZ[a,b,c]

Sébastien PARRATTE[a,b]

Patrick CHABRAND[a,b]

Corresponding author:
Jean-Baptiste RENAULT

Address:

Institut des Sciences du Mouvement UMR 7287

Parc Scientifique et Technologique de Luminy

163, avenue de Luminy

Case Postale 910

F-13288 Marseille Cedex 09 France

Phone number: +33491945242

***Cellphone numbe*r:** +33652136000

E-mail address: jean-baptiste.renault@univ-amu.fr

Affiliations:
a. Aix-Marseille University, CNRS, ISM UMR 7287, 13009 Marseille, France;

b. APHM, Institute for Locomotion, Department of orthopaedics and Traumatology, Sainte-Marguerite Hospital, 13009, Marseille, France

c. Newclip Technics, 44115 Haute-Goulaine, France

d. RLC Systèmes, Marseille, France

Keywords:
Anatomical coordinate system, Surgery planning, Kinematics, 3D imaging, 3D bone model

Word Count:

2197

ACCEPTED MANUSCRIPT

Abstract

Increasing use of patient-specific surgical procedures in orthopaedics means that patient-specific anatomical coordinate systems (ACSs) need to be determined. For knee bones, automatic algorithms constructing ACSs exist and are assumed to be more reliable than manual methods, although both approaches are based on non-unique numerical reconstructions of true bone geometries. Furthermore, determining the best algorithms is difficult, as algorithms are evaluated on different datasets. Thus, in this study, we developed 3 algorithms, each with 3 variants, and compared them with 5 from the literature on a dataset comprising 24 lower-limb CT-scans. To evaluate algorithms' sensitivity to the operator-dependent reconstruction procedure, the tibia, patella and femur of each CT-scan were each reconstructed once by three different operators.

Our algorithms use principal inertia axis (PIA), cross-sectional area, surface normal orientations and curvature data to identify the bone region underneath articular surfaces (ASs). Then geometric primitives are fitted to ASs, and the ACSs are constructed from the geometric primitive points and/or axes. For each bone type, the algorithm displaying the least inter-operator variability is identified. The best femur algorithm fits a cylinder to posterior condyle ASs and a sphere to the femoral head, average axis deviations: 0.12°, position differences: 0.20mm. The best patella algorithm identifies the AS PIAs, average axis deviations: 0.91°, position differences: 0.19mm. The best tibia algorithm finds the ankle AS center and the 1st PIA of a layer around a plane fitted to condyle ASs, average axis deviations: 0.38°, position differences: 0.27mm.

ACCEPTED MANUSCRIPT

Introduction

Progress in the treatment of knee articular pathologies has increased the use of 3D imaging. CT-scans are routinely used by clinicians for diagnostic purposes, surgery planning (Sariali et al. 2012) and patient-specific procedures (Leeuwen et al. 2015; Munier et al. 2017). Associated bone volumetric reconstructions make defining an anatomical coordinate system (ACS) mandatory.

Earlier ACS construction algorithms (Luo 2004; Wu et al. 2002) required manual selection of a small set of landmarks, which is operator-dependent (Victor et al. 2009). To average the errors made during landmark clicking, Fitzpatrick et al. (2007) and Cobb et al. (2008) clicked multiple points on each region of interest (ROI) and derived orientations and center from geometric primitive fitting, centroid or principal inertia axis (PIA) identifications. Kai et al. (2014), Miranda et al. (2010), Olender et al. (2014) and Ho et al. (2012) developed automatic ACS construction algorithms for the femur and tibia, Li et al. (2007) and Rainbow et al. (2013) for the patella, by automatizing ROI selection. However, there is no consensus on the ROIs to select and on the geometries to fit them, and no published algorithm takes for ROI the bone Articular Surfaces (AS). Moreover, although ACSs are constructed on bone models generated from manually segmented 3D images, no study has assessed the influence of this operator-dependent procedure. Our goal is to 1) develop algorithms that automatically identify ASs on the knee bones and use those regions to construct ACSs and 2) evaluate our hypothesis that restricting ROI to ASs makes ACS determination less sensitive to the reconstruction procedure.

To test our hypothesis, we developed 3 algorithms (one per knee bone) that construct subject-specific ACSs by first identifying the ASs. For each of our algorithms, 3 variants are provided. 5 published algorithms were also implemented. All were evaluated on 24 CT-scans, each reconstructed once by 3 different operators.

ACCEPTED MANUSCRIPT

Material & Methods

Bone geometry acquisitions and generations

24 CT-scans, performed for high-tibial-osteotomy surgery planning, were retrieved from the Sainte-Marguerite Hospital database (cf. Supplementary Material-A). The mid-diaphysis of long bones was not acquired. Using Materialise Mimics 19.0, 9 CT-based 3-D bone models were generated by CT-scan, 1 per operator and bone (Figure-1). For the segmentation, masks were created by global grey value thresholding followed by manual corrections when necessary. Reconstruction and smoothing parameters were chosen by each operator. Models were uniformly re-meshed with GMSH 2.16 (Marchandise et al. 2010).

ACS overview

Our algorithms aim at identifying continuous hole-free AS regions of the bone models. Each algorithm identifies the data (points, axes) required to construct an ACS. All geometry fittings are performed using the least-squares method. Algorithms were implemented in Matlab R2016a and available at https://github.com/renaultJB/GIBOC-Knee-Coordinate-System. Algorithms are further detailed in Supplementary Material-B.

Femoral ACS

Femur ACSs are constructed by automatically detecting the femoral head and knee centers (FKC) and a condyle axis (Table-1). First, similar to Miranda et al. (2010), evolution of the cross-section area along the femur 1st PIA (Gonzalez-Ochoa et al. 1998) allows the separation of the distal epiphysis, and gives an initial distalo-proximal axis (Figure-2.A).

The femoral head center is identified using a two-iteration sphere fitting procedure. First, a sphere is fitted to two patches around the most proximal and the most medial vertices of the femoral head. Then,

ACCEPTED MANUSCRIPT

a sphere fitted to all vertices located within 90% and 110% of the initial sphere radius, gives the femoral head center (Figure-2.B).

Condyle Ellipsoids (CE) variant

A medial and a lateral set of vertices are determined thanks to the 3D convex hull of the distal epiphysis (cf. Supplementary Material-B.III.b). The two sets are used to obtain all the condyle ASs, onto which two ellipsoids are fitted. The segment connecting their centers forms the condyle axis and the midpoint of this segment gives the FKC (Figure-2.B).

Posterior Condyle Cylinder (PCC) variant

From the ASs determined with the CE variant, only the parts posterior to the intercondylar fossa are kept, and selection of ASs is refined from surface normal orientations and curvature data. A cylinder is fitted to the posterior condyle ASs. FKC is the barycenter of the ASs projected onto the cylinder axis, which defines the condyle axis (Figure-2.B).

Posterior Condyle Spheres (PCS) variant

Identical to PCC, except two spheres are fitted instead of the cylinder. The segment connecting their centers forms the condyle axis and its midpoint the FKC (Figure-2.B).

Ultimate step of femoral ACS Construction

In each variant, the FKC is the ACS origin. The vector connecting the femoral head center to the FKC is normalized to form the final $\overrightarrow{DP}$ vector. The unit vector of the projection of the condyle axis onto the transverse plan (perpendicular to $\overrightarrow{DP}$) defines the final lateromedial vector $\overrightarrow{LM}$, and its cross product with $\overrightarrow{DP}$ gives the final $\overrightarrow{AP}$ vector to form the ACS basis (Figure-2.C).

ACCEPTED MANUSCRIPT

Tibial ACS

Three variants that automatically detect the tibial ankle and knee centers (TKC) and a condyle axis were developed (Table-2). Our algorithm begins by creating ACS_0, a temporary ACS from PIAs. On the distal tibia, AS elements are identified from curvature data and normal orientations relative to the 1st PIA. The ankle center is defined as the projection of the largest cross-section centroid onto the AS (Figure-3.B). On the proximal epiphysis, the tibial medial and lateral condyle ASs are identified with criteria based on surface curvature data, elements normal orientations and positions in ACS_0 (cf. Supplementary Material B-III.b).

Condyle Articular Surface Centroids (CASC) variant

The centroids of the medial and lateral ASs are identified and connected in a segment, whose midpoint and direction respectively define the TKC and the condyle axis (Figure-3.B).

Ellipse on the Condyle Articular Surface Edges (ECASE) variant

A plane, $\mathcal{P}_{AS}$, is fitted to the combined proximal ASs. The AS vertices are projected onto $\mathcal{P}_{AS}$ and the 2D convex hull of this set of points is generated. Then, an ellipse is fitted to the convex hull vertices. The ellipse center and major axis respectively define the TKC and the condyle axis (Figure-3.B).

Principal Inertia Axis of an Articular Surface Layer (PIAASL) variant

The PIAASL variant identifies a bone layer between two planes parallel to $\mathcal{P}_{AS}$ (Figure-3.B). The layer 1st PIA serves as the condyle axis, while its centroid, projected onto $\mathcal{P}_{AS}$, defines the TKC.

ACCEPTED MANUSCRIPT

Ultimate step of tibial ACS Construction

In each variant, the condyle axis is made orthogonal (as for the femur) to the axis connecting the tibial ankle and knee centers. These two axes plus the TKC define the final ACS (Figure-3.C).

Patellar ACS

The patella resembles a spherical cap, so its 3rd PIA served as an initial AP axis (Figure-4.A), and its vertical ridge can define a distal to proximal (DP) axis. To identify an initial ridge orientation, we used the Rainbow et al. (2013) procedure. Briefly, it consists in finding the most posterior points of evenly separated cross-section outlines taken along the DP axis. Then the DP axis is iteratively reoriented, and the posterior points updated to minimize the standard deviation of their projection on an orthogonal ML axis.

Volume ridge (VR) variant

A non-linear regression is used to remove the points lying on the apex, and DP axis identification is repeated on the remaining points (Figure-4.B). The DP axis is then made orthogonal to the AP axis to define the ACS, the patella centroid being the patella center (PC) (Figure-4.C).

Ridge Line (RL) variant

Alternatively, a line is fitted on the ridge points and the AP axis is made orthogonal to it. The midpoint on the ridge defines the PC (Figure-4.C).

Principal Inertia Axis of the Articular Surface (PIAAS) variant

The AS is identified as the elements within the ridge DP range, using criteria based on their normal orientations relative to the ridge line. The AS PIAs serve as ML, DP and AP axes, while the centroid of the AS completes the definition of the ACS (Figure-4.C).

ACCEPTED MANUSCRIPT

Data analysis

Inter-operator ACS orientation variability of each developed and implemented algorithm (Kai et al. 2014, Miranda et al. 2010 and Rainbow et al. 2013) was evaluated by a global variability angle (GVA) along with per-subject mean ($\overline{AD}$) and across-subject maximal (mAD) paired axis deviations. Axis deviation is the angle between a pair of corresponding ACS basis vectors ($\overrightarrow{AP}$, $\overrightarrow{ML}$ and $\overrightarrow{DP}$).

To calculate GVA all ACS basis were transformed to unit quaternions and for each subject (i), bone (b) and algorithm variant (a) a mean quaternion (Markley et al. 2007) $\boldsymbol{q}_{i,b,a}^{mean}$ was calculated. *GVA* quantifies the global deviation of the orientation of each operator's (k_1) ACS relative to the mean ACS, and is defined by:

$$(b,a) \in \{(Femur, PCC), . , (Patella, VR), \ . , (Tibia, Kai\ et\ al.\ 2014)\}$$
$$i \in [\![1,2,3, \dots ,23,24]\!]$$

$$GVA_{i,b,a} = \frac{2}{3} \sum_{1 \leq k_1 \leq 3} \cos^{-1}\left(\left|\boldsymbol{q}_{i,b,a}^{k_1} \cdot \boldsymbol{q}_{i,b,a}^{mean}\right|\right)$$

$\overline{AD}$ and mAD quantify the difference in orientation between corresponding basis vector for all pairs of operators ($k_1\ and\ k_2$), and are defined by:

$$(b,a) \in \{(Femur, PCC), . , (Patella, VR), \ . , (Tibia, Kai\ et\ al.\ 2014)\}$$
$$i \in [\![1,2,3, \dots ,23,24]\!]$$

ACCEPTED MANUSCRIPT

$$\begin{cases} \alpha_{i,b,a}^{\overline{AD}} = \frac{1}{3} \sum_{1 \le k_1 < k_2 \le 3} \cos^{-1}\left(\overrightarrow{AP_{\iota,b,a,k_1}} \cdot \overrightarrow{AP_{\iota,b,a,k_2}}\right) \\ \alpha_{b,a}^{mAD} = \max_{\substack{1 \le i \le 24 \\ 1 \le k_1 < k_2 \le 3}} \cos^{-1}\left(\overrightarrow{AP_{\iota,b,a,k_1}} \cdot \overrightarrow{AP_{\iota,b,a,k_2}}\right) \\ \beta_{i,b,a}^{\overline{AD}} = \frac{1}{3} \sum_{1 \le k_1 < k_2 \le 3} \cos^{-1}\left(\overrightarrow{LM_{\iota,b,a,k_1}} \cdot \overrightarrow{LM_{\iota,b,a,k_2}}\right) \\ \beta_{b,a}^{mAD} = \max_{\substack{1 \le i \le 24 \\ 1 \le k_1 < k_2 \le 3}} \cos^{-1}\left(\overrightarrow{LM_{\iota,b,a,k_1}} \cdot \overrightarrow{LM_{\iota,b,a,k_2}}\right) \\ \gamma_{i,b,a}^{\overline{AD}} = \frac{1}{3} \sum_{1 \le k_1 < k_2 \le 3} \cos^{-1}\left(\overrightarrow{DP_{\iota,b,a,k_1}} \cdot \overrightarrow{DP_{\iota,b,a,k_2}}\right) \\ \gamma_{b,a}^{mAD} = \max_{\substack{1 \le i \le 24 \\ 1 \le k_1 < k_2 \le 3}} \cos^{-1}\left(\overrightarrow{DP_{\iota,b,a,k_1}} \cdot \overrightarrow{DP_{\iota,b,a,k_2}}\right) \end{cases}$$

Repeatability of origin determination was evaluated with the radii of the minimal bounding spheres (BSR) enclosing the 3 different origins determined by each algorithm on each subject's bones.

We performed two Kruskal–Wallis tests in **R** (R Core Team 2017) on GVA and BSR, to assess whether the algorithms' ACSs were equal. Pairwise algorithm differences were evaluated via a post hoc Dunn's test (Dinno 2017).

Results

All algorithms successfully performed ACS constructions on their corresponding 72 bone models. Detailed results are presented in Table-3 and Table-4, main results being highlighted hereafter.

For the femur, mean algorithm GVAs ranged from 0.08° to 0.39°, with PCC GVA significantly lower than all the others. This translates into lower mean (0.12°) and maximal axis deviations (0.66°) for alpha and

ACCEPTED MANUSCRIPT

beta angle of PCC, as well as the lowest maximal BSR (0.44mm). Algorithm BSRs did not differ significantly.

For the patella, PIAAS mean and maximal axis deviations were between 0.01° and 1.20° lower than those of other algorithms, and its GVA was significantly lower than Rainbow et al. (2013) GVA. The VR and Rainbow et al. (2013) algorithm BSRs were identical and significantly lower than the others.

For the tibia, Kai et al. (2014) and PIAASL had comparable GVAs and BSRs, significantly lower than with other algorithms. PIAASL had the lowest mean (0.05° to 0.39°) and maximal (0.27° to 1.51°) axis deviations.

Variants insensitivity to bone placements are detailed in Supplementary Material-C. While, Joint coordinates system, using the Grood & Suntay (1983) convention, sensitivities to operators are presented in Supplementary Material-E, along with fitting procedures root-mean-square error.

Discussion

We present 3 new automatic algorithms that construct subject-specific ACSs on 3D models of the femur, patella and tibia, and also provide three variants on each algorithm. Together with 5 published algorithms, these were implemented and assessed on 24 subjects. ACSs were not compared among subjects, as we cannot discriminate the effect of the algorithm from the subjects' morphological differences; however, we compared ACSs constructed from the same bones but reconstructed by 3 different operators.

From our results, no algorithm stands out as superior on all criteria (Table-5). However, taking average position (in mm) and orientation variability (in °) as equally important, the best algorithm variants for the femur, patella and tibia are, respectively, PCC, PIAAS and PIAASL.

ACCEPTED MANUSCRIPT

Our main contributions are the automatic identification of AS ROIs, and the first assessment of ACS algorithm sensitivity to operator-dependent bone reconstructions. We show that restricting ROI to AS makes ACS less operator-dependent, our best algorithm variants providing submillimeter and sub-degree variability, lower than the published algorithms we implemented (Kai et al. 2014; Miranda et al. 2010; Rainbow et al. 2013). Two AS characteristics could explain this result. The subchondral bone high x-rays absorption makes ASs less prone to manual correction during segmentation and their smooth geometry limits their sensitivity to reconstruction parameters. We also compared our femur and tibia results to manual method results. Our mean inter-operator axis deviations were 10 to 75% lower than those of Victor et al. (2009), who evaluated the variability of axes derived from manually selected landmarks. Additionally, the *GVA* means of our best tibial and femoral algorithm variants were over 8 times lower than those of Schlatterer et al. (2009).

Least-squares fitting is very sensitive to geometric errors, thus our algorithms contain filtering procedures removing most outliers from identified ASs. Nevertheless, using weighted least-squares could improve the presented algorithms and reduce the found variability.

The presented algorithms were designed for classical morphologies and might fail for pathological ones, especially for the patella which can present a wide range of shape. However, as we presented different variants one's can select the most suited to its application and validate it.

Overall, our findings demonstrate the importance of the choice of both ROI and associated geometries or data. Tibial algorithms based only on identified condyle surfaces display high variability, while those using a larger set of elements yield superior results. To fit the posterior condyle ASs on the femur, considering a cylinder as in Eckhoff et al. (2007), instead of two spheres, significantly improved reliability.

The ACS axes and origins (O) determined by our algorithms make it possible to automatically define the usual anatomical planes for each bone with $(O, \overrightarrow{AP}, \overrightarrow{LM})$, $(O, \overrightarrow{LM}, \overrightarrow{DP})$, $(O, \overrightarrow{DP}, \overrightarrow{AP})$ respectively defining

ACCEPTED MANUSCRIPT

the transverse, frontal and parasagittal planes. This is the first step towards intra-bone measurements, surgical planning and knee kinematic assessment. Using these ACSs, we aim in a future study to identify the planned-vs-achieved position of total knee replacement components.

Conflict of interest statement

None.

Acknowledgements

Work and English revision (Marjorie SWEETKO) funded by Aix-Marseille University.

Appendix-A. Supplementary material

Supplementary information associated with this article can be found in …

Supplementary Material-A: A Microsoft Word file presenting patient information (age, BMI, osteoarthritis grade) and a description of the CT scan protocol used.

Supplementary Material-B: A Microsoft Word file presenting in detail the different steps of the algorithms developed in this study.

Supplementary Material-C: A Microsoft Word file presenting the method used for evaluating the sensitivity of the algorithms to the initial placements of the bones in the CT scan coordinate system. The sensitivity results are also presented in the same file.

Supplementary Material-D: A PDF file of figures to illustrate the differences between the ACSs constructed with the different algorithms, also a list of figures to see the data associated to the minimal, median and maximal GVA for each of the algorithms.

ACCEPTED MANUSCRIPT

Supplementary Material-E: A Microsoft Word file presenting and evaluating the sensitivity of the tibia-to-femur and patella-to-femur joints coordinate systems to the operator's reconstructions. Also, the root-mean-square errors of the used least square fitting procedures are presented in a second part of this material.

ACCEPTED MANUSCRIPT

ACCEPTED MANUSCRIPT

Cobb, J.P. et al., 2008. The anatomical tibial axis: RELIABLE ROTATIONAL ORIENTATION IN KNEE REPLACEMENT. *Journal of Bone and Joint Surgery - British Volume*, 90–B(8), pp.1032–1038.

Dinno, A., 2017. dunn.test: Dunn's Test of Multiple Comparisons Using Rank Sums.

Eckhoff, D. et al., 2007. An ABJS best paper: Difference between the epicondylar and cylindrical axis of the knee. In *Clinical Orthopaedics and Related Research*. pp. 238–244.

Fitzpatrick, C. et al., 2007. A tibial-based coordinate system for three-dimensional data. *Knee*, 14(2), pp.133–137.

Gonzalez-Ochoa, C., McCammon, S. & Peters, J., 1998. Computing moments of objects enclosed by piecewise polynomial surfaces. *ACM Transactions on Graphics*, 17(3), pp.143–157.

Grood, E.S. & Suntay, W.J., 1983. A Joint Coordinate System for the Clinical Description of Three-Dimensional Motions: Application to the Knee. *Journal of Biomechanical Engineering*, 105(2), p.136.

Ho, K.C.T. et al., 2012. Computed tomography analysis of knee pose and geometry before and after total knee arthroplasty. *Journal of Biomechanics*, 45(13), pp.2215–2221.

Kai, S. et al., 2014. Automatic construction of an anatomical coordinate system for three-dimensional bone models of the lower extremities - Pelvis, femur, and tibia. *Journal of Biomechanics*, 47(5), pp.1229–1233.

Leeuwen, J.A.M.J. van et al., 2015. Comparison of planned and achieved implant position in total knee arthroplasty with patient-specific positioning guides. *Acta orthopaedica*, 86(2), pp.201–207.

Li, G. et al., 2007. The coupled motion of the femur and patella during in vivo weightbearing knee flexion. *Journal of biomechanical engineering*, 129(6), pp.937–43.

Luo, C.F., 2004. Reference axes for reconstruction of the knee. *Knee*, 11(4), pp.251–257.

Marchandise, E. et al., 2010. Quality meshing based on STL triangulations for biomedical simulations. *International Journal for Numerical Methods in Biomedical Engineering*, 26(7), pp.876–889.

Markley, F.L. et al., 2007. Averaging Quaternions. *Journal of Guidance, Control, and Dynamics*, 30(4), pp.1193–1197.

Miranda, D.L. et al., 2010. Automatic determination of anatomical coordinate systems for three-dimensional bone models of the isolated human knee. *Journal of Biomechanics*, 43(8), pp.1623–1626.

Munier, M. et al., 2017. Can three-dimensional patient-specific cutting guides be used to achieve optimal correction for high tibial osteotomy? Pilot study. *Orthopaedics and Traumatology: Surgery and Research*, 103(2), pp.245–250.

Olender, G. et al., 2014. Validation of an Anatomical Coordinate System for Clinical Evaluation of the Knee Joint in Upright and Closed MRI. *Annals of Biomedical Engineering*, 42(5), pp.1133–1142.

R Core Team, 2017. R: A Language and Environment for Statistical Computing.

Rainbow, M.J. et al., 2013. Automatic determination of an anatomical coordinate system for a three-dimensional model of the human patella. *Journal of Biomechanics*, 46(12), pp.2093–2096.

ACCEPTED MANUSCRIPT

Sariali, E. et al., 2012. Accuracy of the preoperative planning for cementless total hip arthroplasty. A randomised comparison between three-dimensional computerised planning and conventional templating. *Orthopaedics and Traumatology: Surgery and Research*, 98(2), pp.151–158.

Schlatterer, B. et al., 2009. Skeletal landmarks for TKR implantations: evaluation of their accuracy using EOS imaging acquisition system. *Orthopaedics & traumatology, surgery & research : OTSR*, 95(1), pp.2–11.

Victor, J. et al., 2009. How precise can bony landmarks be determined on a CT scan of the knee? *Knee*, 16(5), pp.358–365.

Wu, G. et al., 2002. ISB recommendation on definitions of joint coordinate system of various joints for the reporting of human joint motion—part I: ankle, hip, and spine. *Journal of Biomechanics*, 35(4), pp.543–548.

ACCEPTED MANUSCRIPT

ACCEPTED MANUSCRIPT

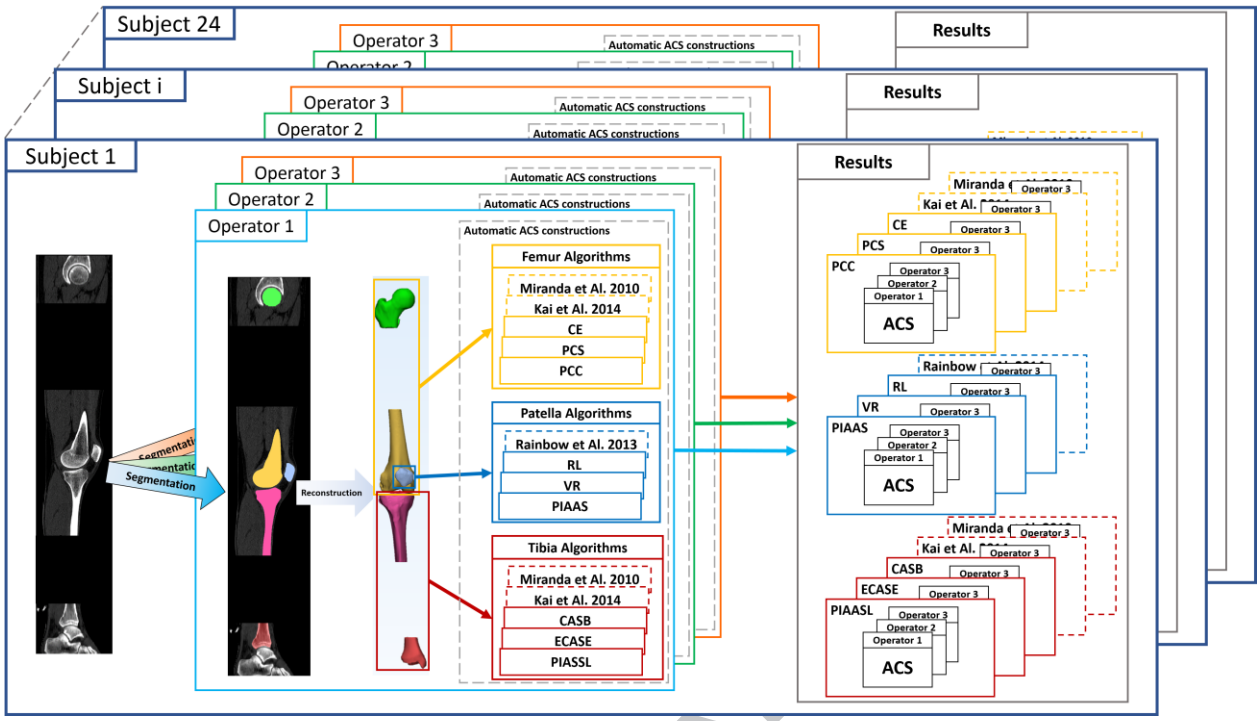

Figure-1. Workflow of the methods applied to the 24 subjects. For each subject, 3 operators independently segmented the CT-scan once. Then each operator reconstructed the 3 knee bones from his own segmentation, yielding 3 bone models per operator. The tibia and femur bone models were composed of two parts, proximal and distal, because the mid-diaphysis of long bone was not acquired during the imaging procedure. Next, the bone models were re-meshed using GMSH to obtain a surface of uniform triangles (target edge length =0.5mm). Then, femur algorithms were applied to the femur model to automatically construct 5 anatomic coordinate systems (ACSs), one per variant. The same procedure was applied to the patella and tibia. In the automatic ACS constructions section, plain lines correspond to the developed 3 variants of each of our algorithms while dashed lines are for the algorithms we implemented from the literature. Finally, the ACSs constructed on the bone models were pooled by algorithm and variants in the results section for each subject for later comparison.

ACCEPTED MANUSCRIPT

ACCEPTED MANUSCRIPT

Variant Label	CE	PCS	PCC
Variant Full Name	Condyle Ellipsoids	Posterior Condyle Spheres	Posterior Condyle Cylinder
Femoral head Center	Center of a sphere fitted on the femoral head		
Condyle ASs	Whole distal femur ASs	Medial and lateral posterior condyle ASs	
Associated primitives	Two ellipsoids	Two spheres	One cylinder
Axis of the condyles	Line connecting the ellipsoid centers	Line connecting the sphere centers	Cylinder axis
Femoral knee center (ACS origin)	Midpoint between the ellipsoid centers	Midpoint between the sphere centers	Centroid of the ASs projected onto the Cylinder Axis

Table-1. Names and brief descriptions of the 3 variants of our algorithm constructing ACSs for the femur.

ACCEPTED MANUSCRIPT

ACCEPTED MANUSCRIPT

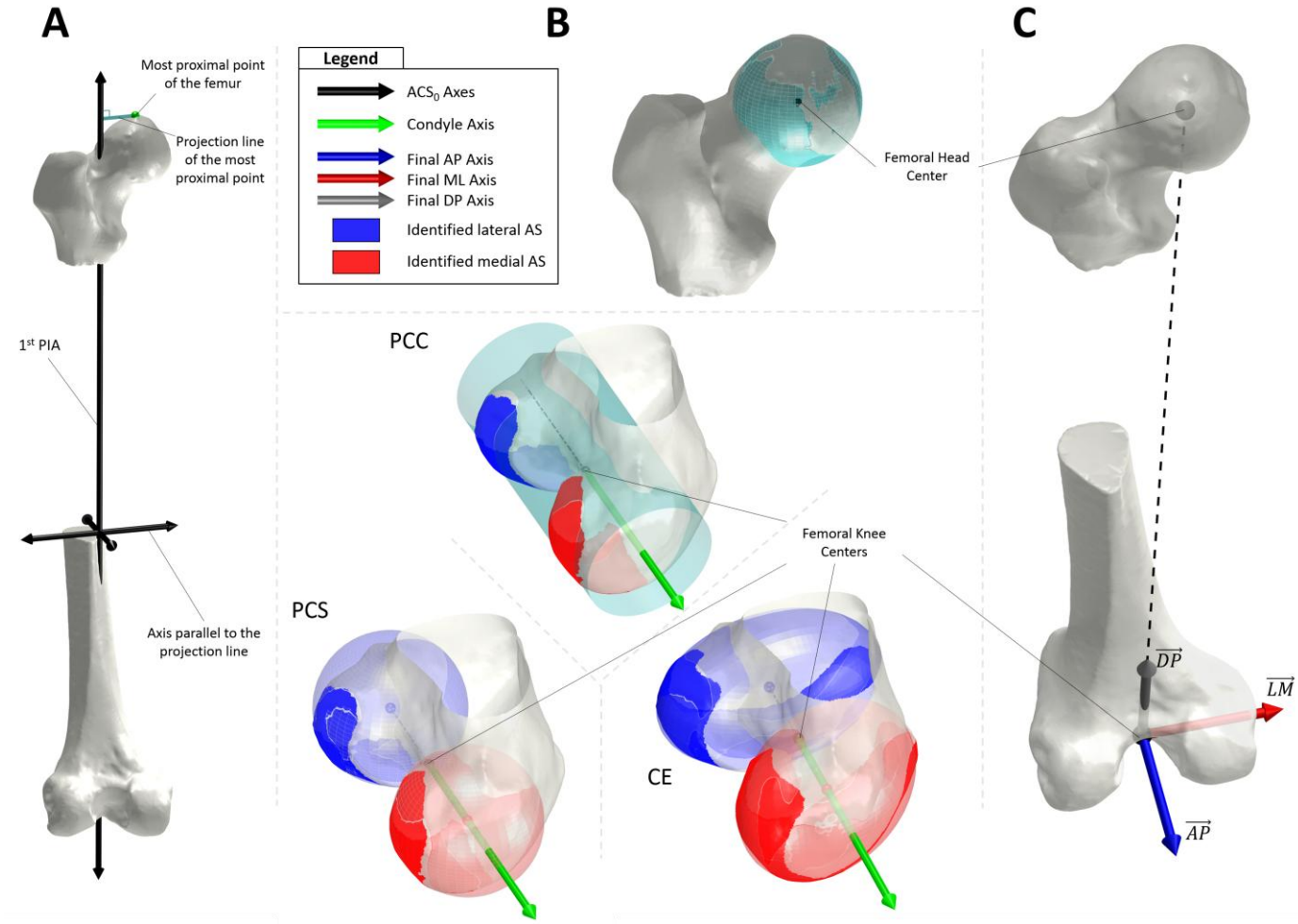

Figure-2. Illustrations of the main steps and features of the 3 algorithm variants we developed to construct an anatomical coordinate system on the femur. (A) Initial coordinate system ACS_0 constructed using the first principal inertia axis of the femur volume and the top of the femoral head. In this coordinate system the approximate positions and orientations of regions of interest are known, this allows for the separation of the distal epiphysis from the rest of the bone and an initial rough identification of the medial and lateral condyles. Those are prerequisites of the subsequent algorithm variants. (B) Top: identification of the femoral head center. Bottom: visual representation of the features of the 3 variants identifying the femoral condyle axis from automatically selected articular surface elements and their different associated geometric primitives. (C) Example of the generic construction of the final right-handed orthogonal ACSs, the procedure for constructing the final ACS from the condyle axis and the axis connecting the femoral knee and head centers is common to all variants. See text and Table-1 *for explanation of the acronyms*.

ACCEPTED MANUSCRIPT

Variant Label	CASC	ECASE	PIAASL
Variant Full name	Condyle Articular Surface Centroids	Ellipse on Condyle Articular Surface Edges	Principal Inertia Axes of Articular Surface Layer
Tibial Ankle Center	Centroid of the largest section of the distal tibia projected onto the distal tibia AS		
Condyle ASs	Two AS regions on the medial and lateral condyles		
Associated primitives		A plane then an ellipse	A plane
Axis of the condyles	Line connecting the centroids of the medial and lateral ASs	Major axis of the ellipse associated with the medial and lateral borders of the ASs	1st PIA of a layer of the tibia around the plane
Tibial knee center (ACS origin)	Midpoint between the centroids	Center of the ellipse	Centroid of the layer projected onto the plane

Table-2. Names and brief description of the 3 variants of our algorithm constructing an ACS on the tibia.

ACCEPTED MANUSCRIPT

ACCEPTED MANUSCRIPT

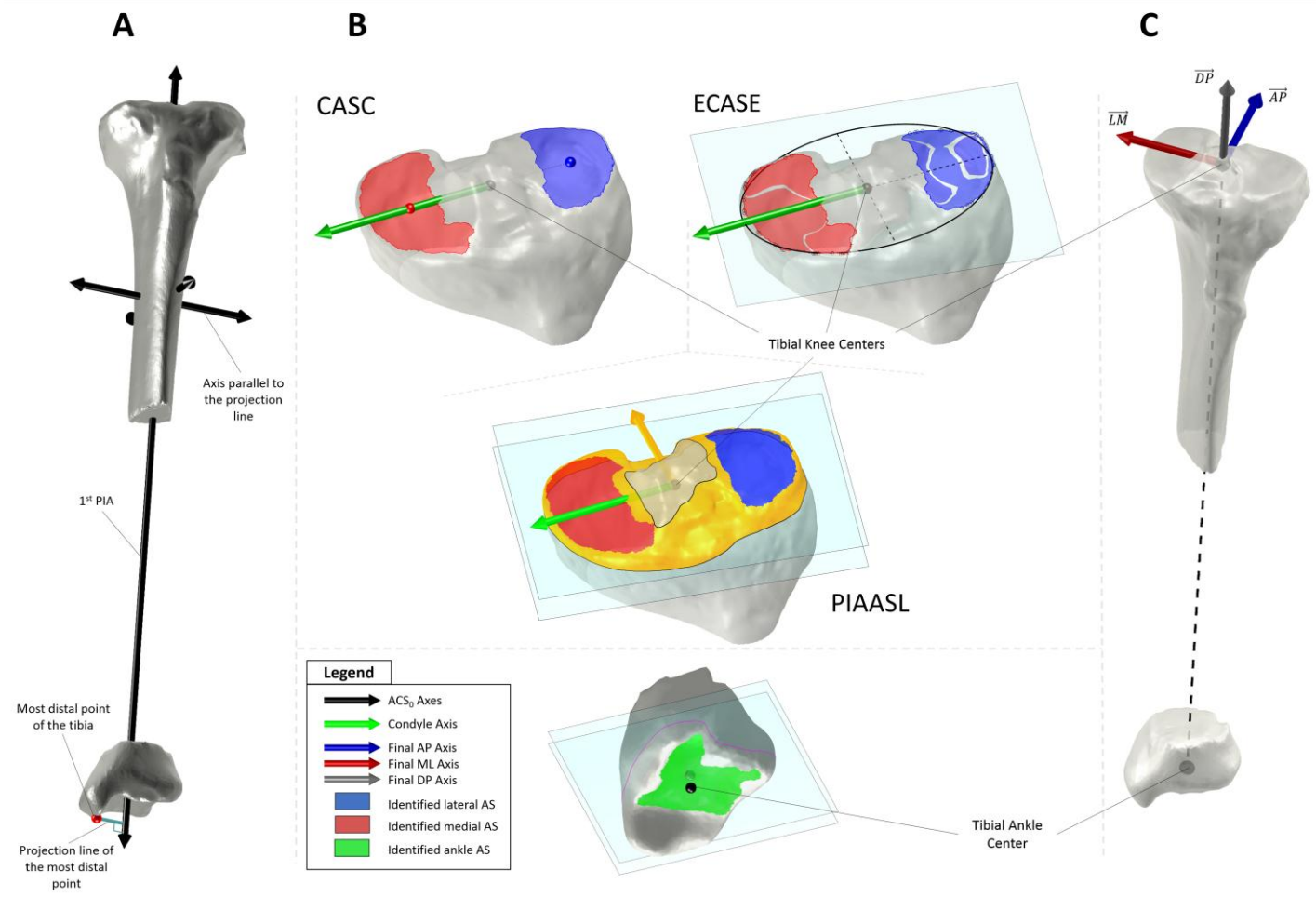

Figure-3. Illustrations of the main steps and features of the 3 variants of the algorithm that constructs an anatomical coordinate system on the tibia. (A) Initial coordinate system ACS_0 constructed using the first principal inertia axis and the summit of the medial malleolus. In this coordinate system the approximate positions and orientations of regions of interest are known, this allows for the separation of the proximal epiphysis from the rest of the bone and an initial rough identification of the medial and lateral condyle articular surfaces. Those are prerequisites of the subsequent algorithm steps that refine the ROI selection. (B) Top: visual representations of the different approaches used by the 3 variants to identify the tibial condyle axis, showing important construction features specific to each method. Bottom: identification of the tibial ankle center. (C) Construction of the final right-handed orthogonal ACSs, the procedure for constructing the final ACS from the condyle axis and the axis connecting the tibial ankle and knee centers is common to all algorithms. See text and Table-2 *for explanation of the acronyms*.

ACCEPTED MANUSCRIPT

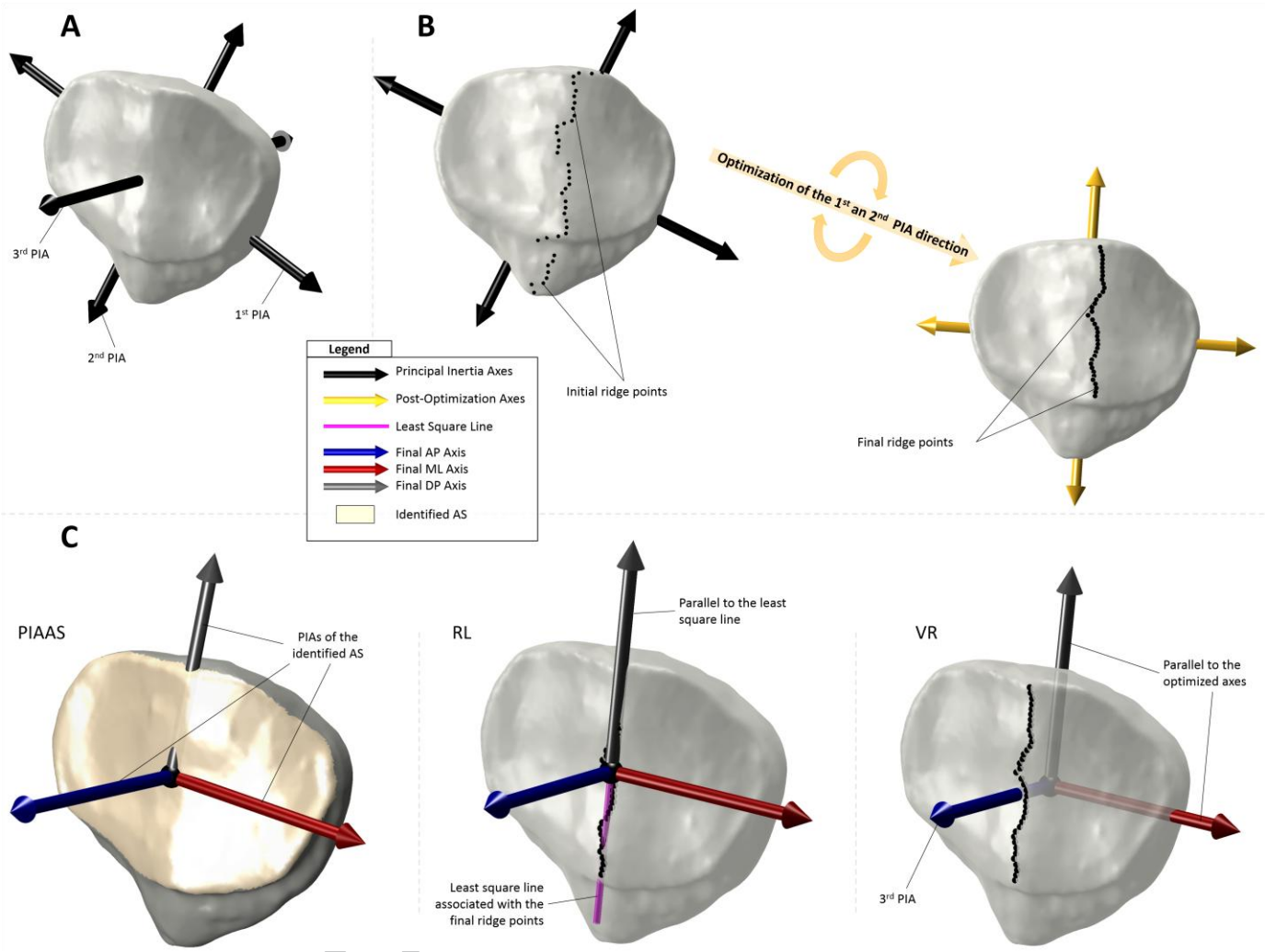

Figure-4. Illustrations of the main steps and features of the 3 variants of the algorithm that constructs an ACS on the patella. (A) Principal inertia axis of the whole patella. Given the patella sphere cap shape, the 3rd PIA is always oriented antero-posteriorly and can be used to identify the vertical ridge on the patella articular surface. (B) Optimization procedure to identify the vertical ridge on the patella AS, at each step the 1st and 2nd PIAs are updated to minimize the deviation of the ridge points when projected on the 1st PIA. (C) Brief description of the construction of the ACS for each variant. See text for explanation of the acronyms.

ACCEPTED MANUSCRIPT

	Methods	Global Variability Angle [°] : GVA mean (SD) max	Axis Deviations [°] Alpha $(\overrightarrow{AP})$ $\overline{AD}$ mean (SD) mAD	Beta $(\overrightarrow{LM})$ $\overline{AD}$ mean (SD) mAD	Gamma $(\overrightarrow{DP})$ $\overline{AD}$ mean (SD) mAD	BSR [mm] mean (SD) max
FEMUR	PCC	0,08 (0,05)	0,12 (0,09)	0,12 (0,08)	0,06 (0,03)	0,20 (0,11)
		0,26	0,66	0,65	0,15	0,44
	PCS	0,15 (0,15)	0,25 (0,24)	0,25 (0,25)	0,05 (0,03)	0,17 (0,12)
		0,63	1,58	1,58	0,15	0,61
	CE	0,16 (0,16)	0,27 (0,24)	0,27 (0,25)	0,05 (0,04)	0,18 (0,26)
		0,80	1,50	1,82	0,25	1,35
	Kai	0,19 (0,14)	0,28 (0,19)	0,27 (0,23)	0,18 (0,20)	0,16 (0,14)
	et al. 2014	0,69	1,18	1,64	1,19	0,67
	Miranda	0,39 (0,13)	0,50 (0,25)	0,66 (0,21)	0,38 (0,13)	0,29 (0,15)
	et al. 2010	0,62	1,50	1,51	0,96	0,63
PATELLA	PIAAS	0,57 (0,25)	0,35 (0,17)	0,93 (0,41)	0,90 (0,42)	0,19 (0,10)
		1,15	0,86	2,65	2,65	0,43
	RL	0,72 (0,42)	0,36 (0,24)	1,21 (0,79)	1,22 (0,79)	0,45 (0,35)
		1,83	1,22	5,09	5,09	1,69
	VR	0,74 (0,43)	0,40 (0,26)	1,21 (0,79)	1,26 (0,81)	0,08 (0,06)
		1,82	1,62	5,09	5,12	0,27
	Rainbow	1,18 (1,37)	0,40 (0,26)	1,21 (0,79)	1,26 (0,81)	0,08 (0,06)
	et al. 2013	1,82	1,62	20,49	20,48	0,27
TIBIA	PIAASL	0,23 (0,15)	0,39 (0,27)	0,39 (0,26)	0,05 (0,04)	0,25 (0,14)
		0,56	1,51	1,51	0,27	0,73
	ECASE	0,68 (0,74)	1,14 (1,10)	1,12 (1,10)	0,27 (0,18)	0,51 (0,40)
		3,83	8,68	8,67	1,26	1,98
	CASC	0,83 (0,53)	1,42 (0,95)	1,40 (0,96)	0,25 (0,14)	0,47 (0,26)
		2,30	6,47	6,47	1,13	1,23
	Kai	0,26 (0,29)	0,41 (0,48)	0,42 (0,48)	0,05 (0,06)	0,27 (0,21)
	et al. 2014	1,19	2,85	2,85	0,49	0,70
	Miranda	0,35 (0,19)	0,58 (0,31)	0,56 (0,29)	0,17 (0,23)	0,30 (0,18)
	et al. 2010	0,82	1,94	1,93	1,75	0,81

Table-3. Overall results, for each bone type and all developed and implemented algorithms, showing Global Variability Angles, Axis Deviations and Radii of minimal Bounding Spheres (BSR) for all subjects.

ACCEPTED MANUSCRIPT

		GVA					BSR				
	p-values	Algorithms					Algorithms				
	VS	PCC	PCS	CE	Kai	Miranda	PCC	PCS	CE	Kai	Miranda
FEMUR	PCC		0,008**	0,003**	0***	0***		0,01**	0,015*	0,029*	0,023*
	PCS	0,008**		0,36	0,12	0***	0,01**		0,19	0,27	0***
	CE	0,003**	0,36		0,21	0***	0,015*	0,19		0,39	0***
	Kai et al. 2014	0***	0,12	0,21		0***	0,029*	0,27	0,3953		0***
	Miranda et al. 2010	0***	0***	0***	0***		0,023*	0***	0***	0***	
	VS	PIAAS	RL	VR	Rainbow		PIAAS	RL	VR	Rainbow	
PATELLA	PIAAS		0,14	0,12	0,013*			0,008**	0***	0***	
	RL	0,14		0,47	0,13		0,008**		0***	0***	
	VR	0,12	0,47		0,15		0***	0***		0,5	
	Rainbow et al. 2013	0,013*	0,13	0,15			0***	0***	0,5		
	VS	PIAASL	ECASE	CASC	Kai	Miranda	PIAASL	ECASE	CASC	Kai	Miranda
TIBIA	PIAASL		0***	0***	0,38	0,03*		0,006	0***	0,49	0,13
	ECASE	0***		0,14	0***	0,01**	0,006		0,41	0***	0,017*
	CASC	0***	0,14		0***	0***	0***	0,4146		0***	0,01**
	Kai et al. 2014	0,38	0***	0***		0,01*	0,49	0***	0***		0,12
	Miranda et al. 2010	0,03*	0,01**	0***	0,01*		0,13	0,017*	0,01**	0,12	

Table-4. Paired comparisons of the different algorithms and variants with a Post hoc Dunn's test for Global Variability Angle (GVA) and minimal Bounding Sphere Radius (BSR) results. Paired comparisons of the algorithms permit their ranking. (: p < 0.05; ** : p < 0.01; *** : p < 0.001). p-Values lower than 0.0001 are displayed as 0 in this table.*

	Algorithms and variants displaying the lowest:			
	Average global orientation variability	**Maximal orientation differences between two operators for all subject**	**Average origin positions variability**	**Maximal origin positions variability of all subjects**
Femur	PCC	PCC	*Kai et al. 2014*	PCC
Patella	PIAAS	PIAAS	VR & *Rainbow et al. 2013*	VR & *Rainbow et al. 2013*
Tibia	PIAASL	PIAASL	PIAASL	*Kai et al. 2014*

Table-5. Presentation of the algorithms displaying the lowest inter-operator variability according to different criteria for each knee bone.